CrystEngComm

Accepted Manuscript

ROYAL SOCIETY OF CHEMISTRY

www.rsc.org/crystengcomm

CrystEngComm

RSCPublishing

ARTICLE

New Growth Modes of Molybdenum Oxide Layered 1D Structures Using Alternative Catalysts: Transverse Mode vs. Axial Mode

Cite this: DOI: 10.1039/x0xx00000x

Received 11th September 2014,
Accepted 18th November 2014

DOI: 10.1039/x0xx00000x

www.rsc.org/

Tao Sheng,[a] Baobao Cao,[bc] Yong Zhang,[d] and Haitao Zhang*[b]

Different from the common metal catalysts (*e.g.*, Au) employed in catalyst-assisted growth of one-dimensional (1D) structures, a variety of molybdenum oxide (MoO_3) layered 1D structures were synthesized using a group of alternative alkali metal based catalysts. In contrast to the sole axial growth mode found in the conventional catalyst-assisted growth, two different growth modes were observed for the MoO_3 1D growth here: transverse growth and axial growth. In the transverse mode, the 1D structures grow perpendicularly to the catalyst-deposition axis with the catalyst particles sitting on the side surfaces of the 1D structures; whereas in the axial mode, the growth direction is along the catalyst-deposition axis. The growth modes were explained by a modified vapor-solid-solid (VSS) mechanism, and factors that affect the growth were explored. Based on the proposed growth mechanism, the growth was extended to a large family of alkali metal based catalysts and hierarchical structures were realized by multiple-growth approaches. This growth mechanism provides a new approach to control the orientation of 1D structures and can be applied to different layered materials.

1 Introduction

Vapor-liquid-solid (VLS) process is the most popular vapor-phase method for the controlled growth of various one-dimensional (1D) microstructures and nanostructures with the assistance of catalyst particles. The VLS mechanism was first proposed and developed in 1960s for the growth of 1D microstructure.[1] With the extensive development of nanotechnology in recent decades, this method has become the most successful and versatile strategy for the synthesis of 1D nanostructures.[2] Based on the similar catalyst-assisted growth mechanism, different processes analogous to the VLS approach have been further developed, including vapor-solid-solid (VSS),[3] solid-liquid-solid,[4] solution-liquid-solid,[5] supercritical fluid-liquid-solid,[6] and supercritical fluid-solid-solid (SFSS).[7] The 1D structure growths via different processes all share two fundamental features. (1) Metal or metal alloy particles are usually used to incorporate the source materials. Noble metals and other transition metals, such as Au, Pt, Ag, Ti, Fe, Ni, and Cu, have been commonly used as catalysts.[2d, 3c] Some low melting temperature metals, like Ga, In, and Sn, have been employed as well.[4c, 8] Although non-metal catalysts, like element semiconductor (Ge)[9] and compounds (Ag_2Se, Ag_2S, and Cu_2S, *etc*.)[10] can also be used for the growth of 1D nanostructures, they are relatively less common compared to the metallic catalysts. (2) As the catalyst particles reach to a supersaturation state, growth occurs at the catalyst-deposition interface leading to the 1D growth along the catalyst-deposition axis as shown in Fig. 1a. The resulting growth is typically an axial growth no matter if it is a tip growth (model I in Fig. 1a) or a root growth (model II in Fig. 1a) or if the catalyst particles are liquid or solid during the growth.[11] Lateral growth (model III in Fig. 1a) of 1D nanostructures has been demonstrated.[12] Though these 1D structures are oriented laterally along the substrate surface, the growth still follows the axial growth mode that the growth front is the catalyst-deposition interface and the growth direction is along the catalyst-deposition axis.

Orthorhombic molybdenum trioxide (α-MoO_3) has an anisotropic layered structure with strong ionic and covalent bonding within the (010) layers but weak van der Waals interactions between the (010) layers.[13] α-MoO_3 has potential applications in a wide range of areas of electrochromism and photochromism,[14] lubricants,[15] photocatalysts,[16] and gas sensors.[17] Moreover, as a layered hosting material, α-MoO_3 has enabled improved performance in Li-ion[18] and Na-ion battery.[19] Various MoO_3 nanostructures have been synthesized through solution-based hydrothermal procedures[20] and chemical vapor transport/deposition approaches,[21] including nanowires, nanobelts, nanoflowers, prims-like rods, and nanoribbons. So

far, the investigation on the catalyst-assisted growth of MoO_3 1D nanostructures is still rare. The assistance of Au in vapor deposition only altered the orientation[21f] or served as preferred nucleation sites[22] of the 1D nanostructures rather than promoting the growth of the nanostructures.

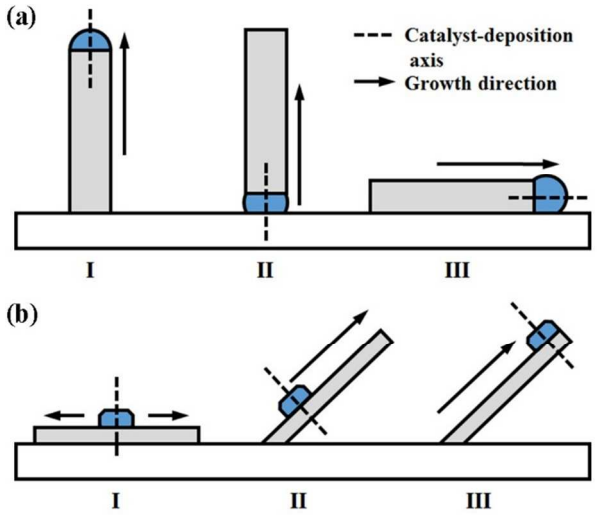

Fig. 1 Comparison of different growth modes for the catalyst-assisted growth of 1D structures. (a) Conventional axial growth mode with tip growth (model I), root growth (model II), and lateral growth (model III). The growth direction for the axial growth mode is parallel to the catalyst-deposition axis. (b) New transverse growth mode with lateral growth (model I) and vertical growth with catalyst particles at different locations along the 1D structures (model II and III). The growth direction for the transvers growth mode is perpendicular to the catalyst-deposition axis.

In this study, instead of the common metal catalysts, alternative catalysts were employed in the growth of MoO_3 1D structures, including sodium or potassium compounds (*e.g.*, hydroxides, halides, and carbonates, etc.) and even alkali metal containing substrates (*e.g.*, glass, indium-tin-oxide (ITO) coated glass, and mica). The growth is greatly enhanced with the presence of the catalysts producing 1D structures with different morphologies, including forked nanoplates, extra-long nanobelts, millimeter-long microbelts, and microtowers. The growth mechanism of the 1D structures was identified as dominated by the VSS process. Most importantly, different from the conventional VSS and similar mechanisms, the 1D growth of MoO_3 here follows two different growth modes: transverse growth and axial growth. The new transverse growth is demonstrated with the growth of MoO_3 nanoplates, nanobelts, and microbelts. In the transverse growth shown in Fig. 1b, the 1D structures grow perpendicular to the catalyst-deposition axis with catalyst particles sitting on different locations (models I-III in Fig. 1b) along the side surfaces of the 1D structures. On the other hand, the MoO_3 microtowers show a conventional axial growth along the catalyst-deposition axis. These growth modes were explained by a modified VSS growth mechanism, and factors that affect the growth were explored. Based on the growth mechanism, the growth was extended to a large family of alkali metal based catalysts and hierarchical structures were generated using multiple-growth approaches.

2 Experimental

2.1 Reactants and substrates

Molybdenum powers (Mo, Alfa Aesar, 99.9%) were used as the source material for the growth of molybdenum oxide. Different reactants were used as the catalytic materials in this study including powders of sodium hydroxide (NaOH, Fisher Scientific, 99.8%), sodium iodide (NaI, Alfa Aesar, 99.9%), potassium iodide (KI, Alfa Aesar, 99.9%), sodium carbonate (Na_2CO_3, Alfa Aesar. 99.95%). All reactants were used as received without further processing.

Silicon (100) substrates (*p*-type, University Wafers) were mainly used in the experiments. The substrates were first cut into 10 mm by 25 mm pieces and ultrasonically cleaned with acetone and ethanol for 15 min (Branson 1510R-MTH, Fisher Scientific), each followed by blow-drying with nitrogen gas. After above cleaning, the substrate surfaces were hydrophobic. To render hydrophilic substrate surfaces, the substrates were then treated with oxygen plasma (Plasma-Preen 862, Kurt J Lesker) for 3 min. For the catalysts-assisted experiments, the hydrophilic Si substrates were drop-cast with NaOH (or KI, Na_2CO_3) solution (54 μL, 10 mM) and air dried in a chemical fume hood. Other alkali ions containing substrates, such as soda-lime-silica glass (microscope slide, Fisher Scientific) and indium tin oxide (ITO) coated glass (Delta Technologies, 25Ω/□), were cleaned by the same routine except the absence of plasma cleaning and subsequent aqueous solution dipping. Mica (Ted Pella, grade V2, #52-25) was cleaved right before growth without other treatment.

2.2 Synthesis

The growths were performed in a home-made hot-wall chemical vapor deposition (CVD) system. The detailed setup has been reported elsewhere.[23] In a typical synthesis, Mo powders were loaded at the center of the reaction chamber with receiving substrate placed at the downstream. The reaction chamber was first pumped down to ~10 mTorr, and then brought up to ~ 200 mTorr with 10 sccm (standard cubic centimeter per minute) O_2 and 10 sccm Ar. The heating temperature at the center was ramped up to 800 °C in 30 min and lasted for 120 min. Then the heating power was turned off and the chamber was allowed to naturally cool down to room temperature. During the growth, the growth temperature along the substrate was about 620 °C to 300 °C, according to the temperature profile measured at atmosphere pressure.

2.3 Material Characterization

The morphology and composition of the as-synthesized samples were analyzed by scanning electron microscopy (SEM, JEOL JSM-6480) and energy dispersive X-ray spectroscopy (EDS, Oxford Instrument INCA). Crystal structures were characterized using X-ray diffraction (XRD, PANXpert X'pert Pro MRD with Cu Kα radiation at λ = 1.5418 Å) and transmission electron microscopy (TEM, JEOL JEM-2100

LaB_6 operated at 200 kV). Optical measurements were performed using a confocal micro-Raman system (Horiba Scientific, Labram HR800) in backscattering configuration. Laser power approximately 0.3 mW at 532 nm was used with a 100× objective lens. The spectral resolution is about 1 cm^{-1}. Optical absorption spectra were recorded using ultraviolet-visible (UV-vis) spectrophotometer (Schimadzu, UV2600Plus) in transmission mode. The as-synthesized sample was removed from substrates by ultra-sonication in ethanol for 15 sec. The dispersion was left for 12 h to ensure enough sedimentation so that the dispersion became transparent under the unaided eye. The dispersion was then transferred into one 10 mm quartz cuvette (Thorlabs, W005654) for absorption measurement.

3 Results and discussion,

3.1 Synthesis and characterization of layered 1D structures

1D MoO_3 structures were found to grow over a wide range of substrate growth temperatures from ~ 525 °C to 300 °C for both the growth without catalysts and the growth with NaOH catalysts. Figure 2 shows a comparison of the morphology differences between the non-catalyst growth (Fig. 2a) and the catalyst-assisted growth (Fig. 2b-f) with scanning electron microscopy (SEM) images. For the non-catalyst growth, nanoplates with a rectangular shape were formed with a length of tens of microns, width of several microns, and thickness of hundreds of nanometers. The dimension of the rectangular nanoplates varies with growth temperatures (shown in Fig. S1 in Supporting Information). Typical rectangular nanoplates grown at ~ 490 °C with straight edges are shown in Fig. 2a, and the inset shows the nanoplates have a booklet-like feature consisting of nanometer-thick layers similar to the MoO_3 nanostructures in previous reports.[22, 24] On the other hand, the catalyst-assisted growth resulted in 1D structures with different morphologies. First, the MoO_3 deposition with catalysts yielded a two-tier structure with different ultra-long 1D structures, such as nanobelts (Fig. 2d), microbelts (Fig. 2e), and microtowers (Fig. 2f), grown on top of a dense array of nanoplates (Fig. 2c). This two-tier structure indicates that there are two stages for the catalyst-assisted growth of MoO_3. As shown in Fig. 2b, ultra-long nanobelts (bright features) were grown on top of a nanoplate array (dark background indicated by the square). A close-up view of the nanoplate array in Fig. 2c shows the nanoplates grown at ~525 °C with NaOH catalysts have a distinctive forked feature and larger sizes compared to those rectangular ones in Fig. 2a grown without catalysts. Fig. 2d shows ultra-long nanobelts with a length of hundreds of microns up to about one millimeter at the growth temperature of ~ 490 °C. At the growth temperature of 390 °C, microbelts with a thickness of microns and length of millimeters appeared with dense circular or semicircular nanoflakes (inset of Fig. 2e) condensed on the side surfaces of the belts. As the substrate growth temperature further deceased to ~ 300 °C at downstream, tower-like structures (Fig. 2f) with micron-sized diameters and lengths were formed at the downstream end of the substrate. The microtowers are stacking structures of quasi-circular layers with tapered tips or flat tops (Fig. 2f and its inset).

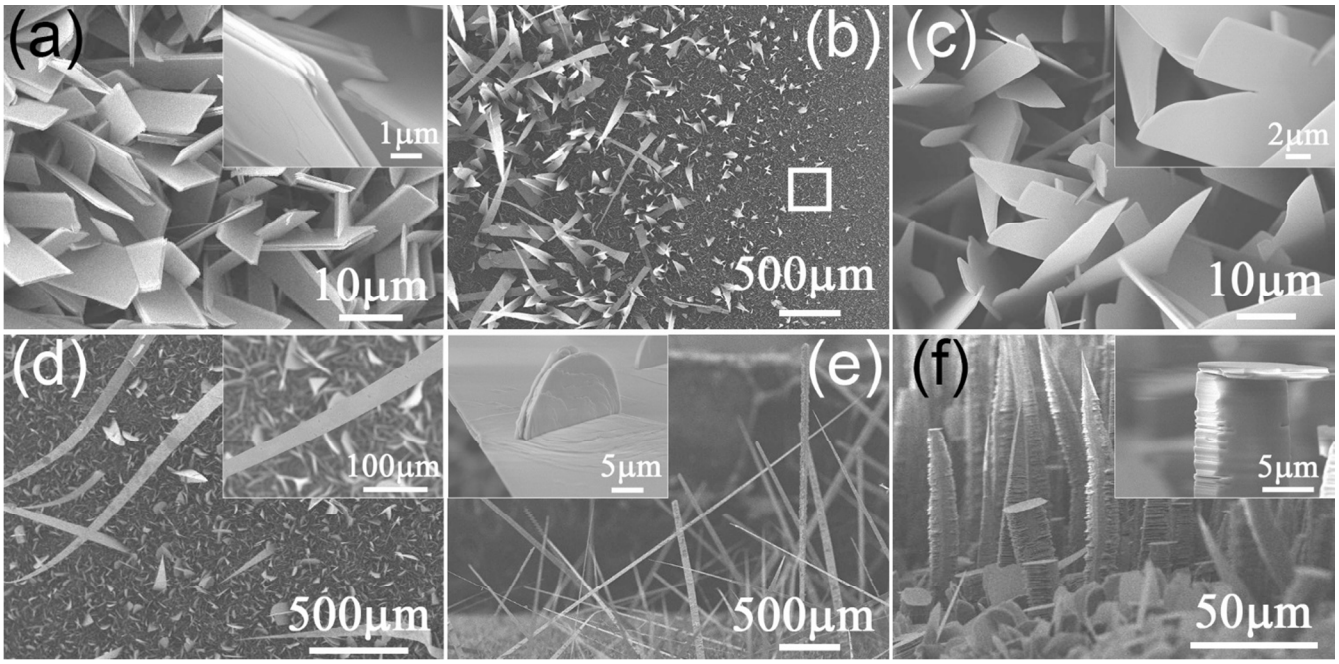

Fig. 2 Effect of alkali metal-based catalysts on the morphology of MoO_3 depositions. (a) SEM image of rectangular nanoplates grown at ~ 490 °C without any catalysts. (b-f) SEM images of different morphologies grown with NaOH catalysts: (b) nanobelts grown on top of dense array of nanoplates grown at ~ 525 °C, (c) close-up view

of the forked nanoplates from an area indicated by the square in Fig. 2b, (d) long nanobelts at ~ 490 °C, (e) side-view of ultra-long microbelts at ~ 390 °C, and (f) side-view of microtowers at ~ 300 °C. Insets show detailed features of different MoO_3 structures.

The crystal structures of the as-synthesized specimens were characterized with XRD for the non-catalyst growth (Fig. 3a) and catalyst-assisted growth (Fig. 3b). The XRD patterns for both growths match closely the standard pattern of the orthorhombic α-MoO_3 phase (ICDD PDF # 04-012-8070, a = 3.9616 Å, b = 13.8560 Å, and c =3.6978 Å). The calculated lattice parameters are a = 3.963 Å, b = 13.882 Å, and c = 3.701 Å for the non-catalyst growth and a = 3.967 Å, b = 13.865 Å, and c = 3.701 Å for the catalyst-assisted growth, coinciding with the standard data. No other phases were found from XRD spectra for both specimens. This result indicates that if there are any catalyst phases present in the catalyst-assisted specimen, they must be in a very small amount below the detection limit as compared to the amount of the MoO_3 phase. Figure 3b for the catalyst-assisted growth demonstrates dominant diffraction peaks of (020), (040), and (060) showing a strongly preferred orientation, which may be attributed to the ultra-long 1D structures (Fig. 2d-f) with layered structures oriented preferably parallel to the substrate surface and some nanoplates grown laterally along the substrate surface during the early growth stage (discussed later in the text). The α-MoO_3 phase was also confirmed by TEM on individual 1D structures. Figure 3c shows low magnification TEM image of a rectangular nanoplate grown without catalysts and its selected area electron diffraction (SAED) pattern. The nanoplate was exfoliated by ultra-sonication in acetone solution to reduce its thickness to get high-resolution TEM (HRTEM) image, hence the nanoplate was broken into a smaller piece. The SAED pattern in [010] axis (Fig. 3c) and the HRTEM image (Fig. 3d) show the nanoplate has a (010) top surface and two orthogonal edges along [100] and [001] respectively. For the catalyst-assisted growth, Fig. 3e and Fig. 3f-g confirm both the forked nanoplate (without exfoliation) and the nanobelt have a (010) top surface and a growth direction of [001], while Fig. 3h reveals the microtower is a layered structure of (010) layers stacking along a [010] direction. Lattice measurements in Fig. 3d and 3g indicate a planar distance of 0.38 nm for (100) planes and 0.36 nm for (001) planes. These values are slightly smaller than the standard data for α-MoO_3 and the results from XRD measurements. This deviation in lattice parameters may be due to the small error in TEM measurements and the lattice distortion and change from the electron beam irradiation during the TEM examination.[25] These results reveal that all the as-synthesized 1D structures have a layered structure consistent with the anisotropic crystal structure of the α-MoO_3.[13b, 26]

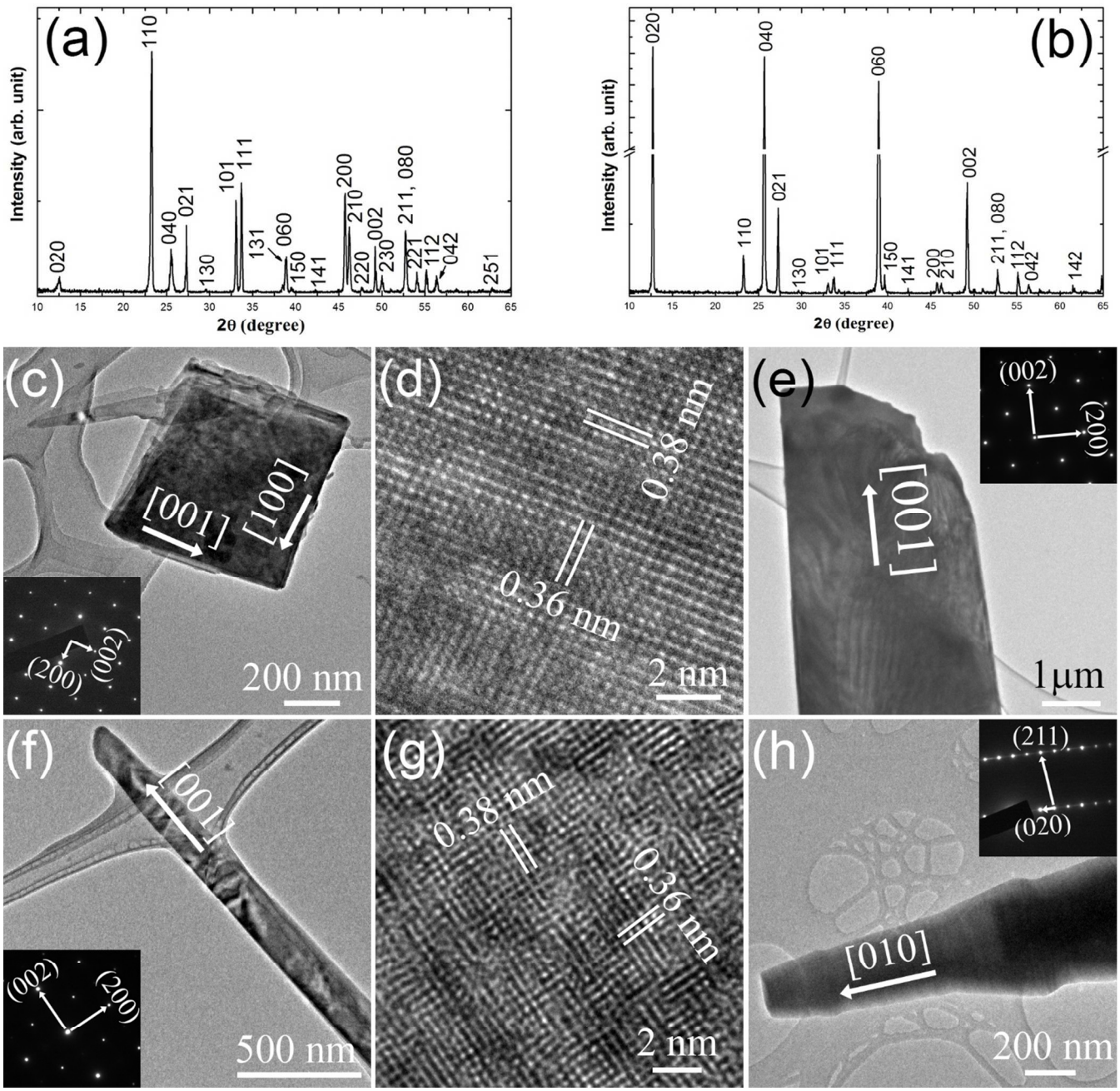

Fig. 3 XRD spectra of (a) a specimen grown without catalysts and (b) a specimen grown with NaOH catalysts. (c) Low-magnification TEM image and (d) HRTEM image of nanoplate grown without catalyst. (e-h) Various 1D structures grown with NaOH catalysts: low-magnification TEM images of (e) forked nanoplate, (f) nanobelt, and (h) microtower, and HRTEM image of (g) nanobelt. Insets show SAED patterns of different MoO_3 1D structures.

3.2 Growth evolution and mechanism

The growth process of the 1D MoO_3 rectangular nanoplates without catalysts is similar to the reported CVD growth of 1D WO_3 nanowires,[23a] that the refractory metal powders (*e.g.* Mo and W) were oxidized by heating in an oxygen ambient, oxide vapors were then evaporated and transported downstream forming deposition on the substrate at lower temperature. Therefore, the non-catalyst growth of these MoO_3 rectangular nanoplates can be explained by the vapor-solid (VS) growth mechanism,[27] as proposed in other vapor phase deposition of MoO_3 belt structures.[21c, 21e] On the other hand, as shown in Fig. 2, with the addition of NaOH catalysts, the growth of MoO_3 is greatly enhanced and has two growth stages. To reveal the growth mechanism and the role of the catalysts in the growth, evolution studies were performed on the early stage growth of the forked nanoplates and the second stage growth of the different ultra-long 1D structures.

MoO_3 has a high vapor pressure before the source heating temperature reach to 800 °C, for example, its vapor pressure is

~ 76 mTorr at 661 °C.[28] The deposition formed during both the temperature ramping and cooling steps will become dominant when the growth time is small. Therefore, the growth evolution for the early stage of the MoO_3 growth cannot be simply performed by reducing the growth time at 800 °C. The production of oxide vapor in our experiments is limited by the oxidation of Mo powders, so the amount of MoO_3 deposition at the early growth stage can be controlled by adjusting the O_2 flow rate. To reveal the initial growth with small amount of MoO_3 deposition, a series of experiments (as shown in Fig. 4) were performed at different O_2 flow rates of 0.1 sccm, 1 sccm, 3 sccm, and 10 sccm with a constant growth time of 15 min. To identify the phase change during the growth, micro-Raman spectroscopy was performed on these specimens. The phases were identified by matching the Raman spectra with the Raman patterns reported in literatures.[29] The Raman spectra of molybdenum oxide and sodium molybdates are featured with multiple strong peaks located in the high-frequency region from 800 to 1000 cm^{-1}. In this region, MoO_3 phase shows two peaks with the strongest one at ~ 820 cm^{-1}; $Na_2Mo_2O_7$ phase exhibits five peaks with the strongest one moving to ~ 937 cm^{-1}; whereas $Na_2Mo_4O_{13}$ phase has even more peaks at about 819, 841, 898, 915, 962, 970, and 995 cm^{-1}, respectively. Detailed matching and comparison of the Raman peaks between the present work and previous reports are provided in Table S1. At low O_2 flows, *e.g.* 0.1 sccm (Fig. 4a) and 1 sccm (Fig. 4d), the MoO_3 deposition shows an island growth with micron-sized particles. The islands grown at 0.1 sccm O_2 was identified as the $Na_2Mo_2O_7$ (*i.e.*, $Na_2O{\cdot}2MoO_3$) phase according to its Raman pattern in Fig. 4b. As the O_2 flow increased to 1 sccm, the deposition developed to be the $Na_2Mo_4O_{13}$ (*i.e.*, $Na_2O{\cdot}4MoO_3$) phase with small amount of MoO_3 as revealed by the Raman spectrum in Fig. 4e. This result shows after the formation of $Na_2Mo_4O_{13}$, MoO_3 started to precipitate underneath the catalyst material. Element analyses in Fig. 4c and 4f using EDS also confirm the existence of Mo, Na and O in both island depositions. (Note: the Si signals were from the substrates.) With further increase of O_2 flow to 1 sccm (Fig. 4g) and 10 sccm (Fig. 4j), the deposition has a morphology of triangular-like particles on top of 1D forked plates. Micro-Raman measurements were carried out on individual particles and plates as shown in Fig. 4h and 4k. For both specimens, the particles were found remaining in the $Na_2Mo_4O_{13}$ phase with small amount of MoO_3 phase from the background, but the plates were identified as the MoO_3 phase. EDS spectra (Fig. 4i and 4l) also confirmed the particles had Mo, Na and O, while only Mo and O were present in the plates showing the growth of MoO_3 plate structures. As shown in Fig. 4g and 4j and previously in Fig. 2, unlike the rectangular nanoplates grown without catalysts, the nanoplates grown with catalysts are highly forked plates with wavy or angled high Miller index surfaces (*e.g.*, in forms of [*h0l*]) off the [001] planes). With the unsaturated chemical bonds of the surface atoms, these high index surfaces could serve as the growth fronts resulting in a fast growth along the <001> directions.[21a] The forked morphology may be induced by the Na^+ doping in the MoO_3 matrix. The Na^+ doping in MoO_3 was reported to be able to increase the mobility of Mo^{6+} ions through the MoO_3 lattices.[30] This property may also contribute to the enhanced growth of MoO_3 1D structures with NaOH catalysts. However, the absence of Na signals in the EDS spectra (Fig. 4i and 4l) from the forked MoO_3 nanoplates indicates the Na^+ doping level in MoO_3 is lower than the detection limit of 0.01wt% for the EDS.[31]

CrystEngComm RSCPublishing

ARTICLE

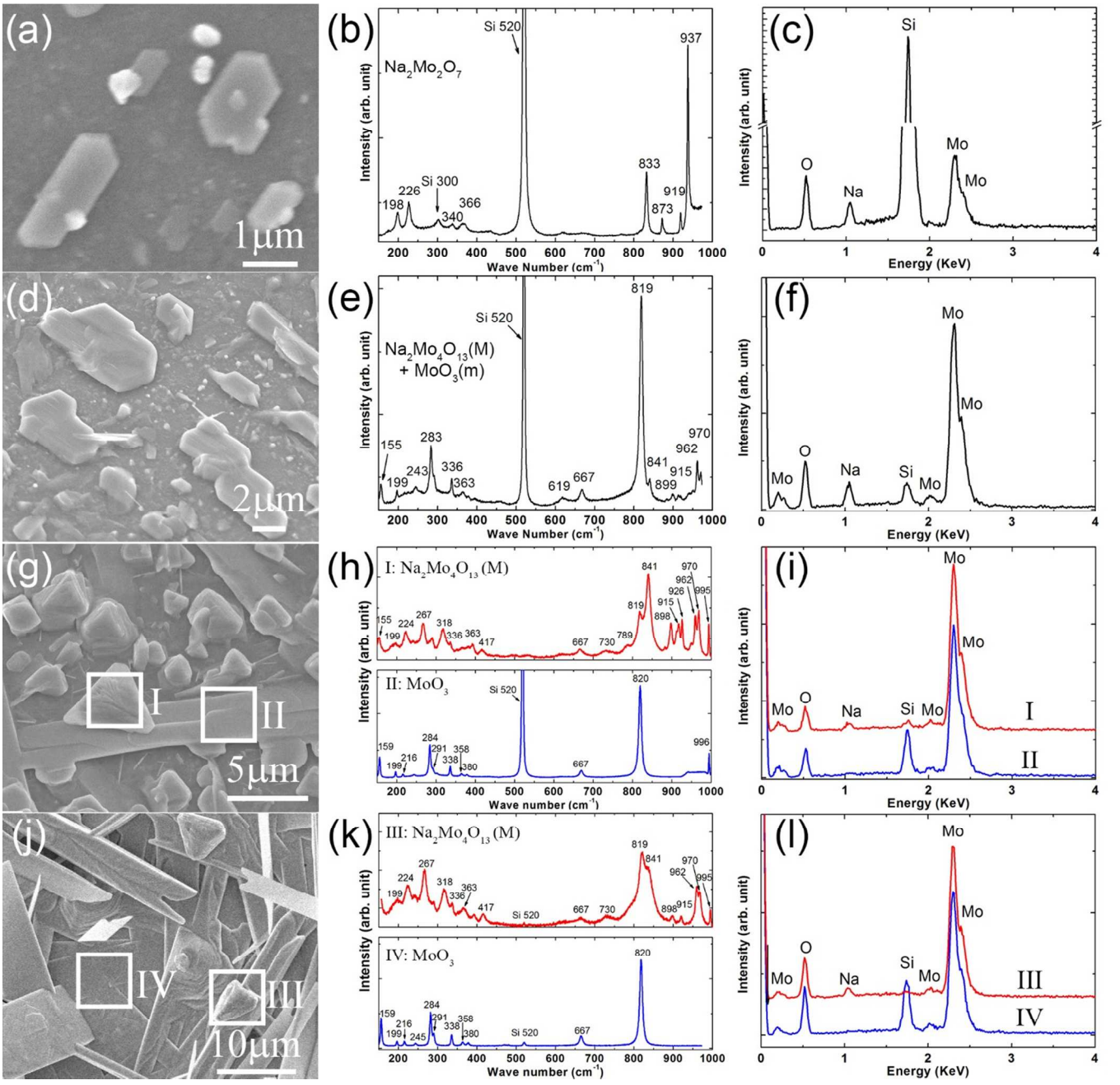

Fig. 4. Growth evolution of the early stage of catalyst-assisted growth of MoO_3 1D structures: SEM images, micro-Raman spectra, and EDS spectra of the specimens grown for 15 min with different O_2 flows of (a-c) 0.1 sccm, (d-f) 1 sccm, (g-i) 3 sccm, and (j-l) 10 sccm. The chemical phases are labeled in corresponding Raman spectrum, with M denotes majority, and m for minority.

The observed compositional and phase evolutions match the phase diagram of Na_2MoO_4-MoO_3 binary system shown in Fig. 5a.[32] During the growth, the NaOH catalysts can directly react with MoO_3 vapor or decompose into Na_2O[33] and then reacts with MoO_3 vapor forming sodium molybdates.[30] As shown in Fig. 5a, at a typical growth temperature the sodium molybdate

phase changes from Na_2MoO_4 to $Na_2Mo_2O_7$, and then to $Na_2Mo_4O_{13}$ with the increase of the supply of MoO_3 vapor. With further increase of the MoO_3 composition, MoO_3 solid phase starts to nucleate and grow while the $Na_2Mo_4O_{13}$ phase remains the same. Since the growth temperature range of 525 – 300 °C (shadowed area on Fig. 5a) for the MoO_3 deposition is mainly below the lowest eutectic temperature of ~ 507 °C, the majority of the growth of the MoO_3 plates can be explained as a VSS process. However, the temperature profile of the CVD system was measured at atmosphere pressure without gas flows, while the growth was carried out at low pressures with continuous gas flows. The actual growth temperature on the substrate could be higher than the one indicated by temperature profile, depending on the pressure and flow rate.[34] The heat transfer along the substrate may also affect the temperature on the substrate. Thus, the VSS mechanism here may be the dominant process for the catalyst-assisted growth but the VLS mechanism cannot be totally ruled out, especially for the high growth temperature area. Different from the conventional VSS (and VLS) growth, the most significant feature of the MoO_3 nanoplate growth here is its transverse growth mode in which the growth direction is perpendicular to the catalyst-deposition axis. To explain this unique transverse growth, we propose a modified VSS growth mechanism for the transverse growth of MoO_3 1D structures based on the spreading behavior of MoO_3. It has been reported in literatures that MoO_3 can spontaneously spread over the surface of supports (*e.g.*, Al_2O_3, SiO_2, TiO_2, and Au) to form a monolayer or submonolayer at a temperature (*e.g.*, 257 °C) well below its melting point of 795 °C.[35] The transport of Mo oxide species during the spreading can occur over macroscopic distances, *e.g.*, several hundred microns depending on the temperature and time of the thermal treatments. This strong spreading behavior can be explained by the solid-solid wetting process, in which the dominant driving force is the decrease in total surface free energy.[35a] Although the detailed transport mechanisms of the spreading are still under debate, it was suggested that the high mobility of the Mo oxide species on substrates and MoO_3 islands can promote the spreading and the ambient gases could further enhance the spreading.[35a, 35c-e] Therefore, the steps of the modified VSS growth are proposed and depicted in Fig. 5b: (i) the catalysts react with MoO_3 vapor forming molybdate particles, (ii) MoO_3 starts to nucleate and form a wetting layer between the particles and the substrate, (iii) as growth continues, more MoO_3 precipitates and spread laterally yielding the transverse growth of the nanoplates, and (iv) when the nanoplates grow longer and denser, they start to grow upward forming a nanoplate array. Detailed atomic processes involved in the nanoplate growth are illustrated in Fig. 5c. Several pathways can contribute to the growth of MoO_3 nanoplates. MoO_3 vapor is accommodated into the molybdate particles and supersaturated MoO_3 in the molybdate catalysts will precipitate (pathway I). The precipitated MoO_3 may grow at the catalyst-deposition interface (pathway II), or spread along the top surface of MoO_3 (010) and grow at the edges (pathway III). With the strong spreading property of MoO_3, the growth via pathway III is dominant in our experiments resulting in the transverse growth of the nanoplates. Besides the VSS processes, the transverse growth can be further enhanced via the VS processes: (pathway IV) MoO_3 vapor directly condenses onto the growth fronts forming deposition, and (pathway V) MoO_3 vapor adsorbs and diffuses on the (010) surface and produces deposition at the growth fronts. Therefore, the MoO_3 nanoplate growth with alkali metal based catalysts can be explained by the VSS growth mechanism enhanced with the VS mechanism. The transverse growth mode is attributed to the strong spreading capability of MoO_3. Growth also using alkali metal based catalysts (*e.g.*, KOH and KI) has been reported with $K_2W_4O_{13}$ nanowires and WO_3 nanoribbons and nanosheets.[36] However, only the growth temperature slightly higher than the eutectic temperature was investigated in these reports, and the growth was generally explained by the VLS mechanism. No detailed observation of the location and morphology of the catalyst particles was provided. No transverse growth mode was claimed in these reports and this may be due to the differences in spreading properties between the MoO_3 and the WO_3 or $K_2W_4O_{13}$.

CrystEngComm RSCPublishing

ARTICLE

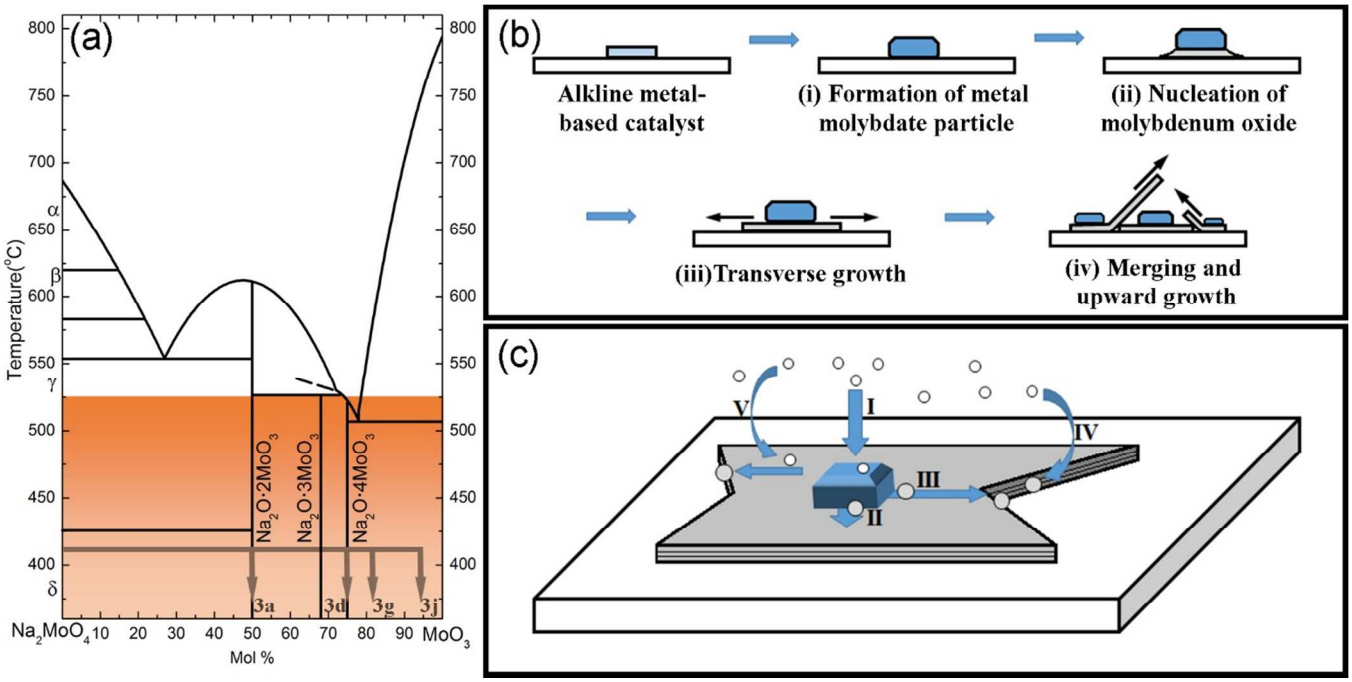

Fig. 5 (a) Na_2MoO_4-MoO_3 binary phase diagram[32] with growth steps indicated showing the early stage evolutions of compositions and phases in Fig. 4. Shadowed area shows the range of the growth temperature. (b-c) Schematic illustrations of (b) growth steps of the VSS growth of MoO_3 nanoplates and (c) atomic processes involved in the VSS mechanism.

Growth evolution of the second stage of the MoO_3 growth was investigated at a constant O_2 flow rate of 10 sccm with different growth time of 30 min, 60 min, and 90 min as shown in Fig. 6. Compared to the 15 min growth shown in Fig. 4j, dense arrays of MoO_3 forked nanoplates with a length of hundreds of microns were formed covering the substrate areas at different temperatures (Fig. 6a-d). With the increase of the growth time, these nanoplates kept growing and became larger, longer, and denser. Ultra-long 1D MoO_3 structures started to grow on top of the nanoplate arrays. For the growth time of 60 min (Fig. 6e-h), ultra-long nanobelts appeared on top of the nanoplates at the vicinities of 445 °C (Fig. 6f) and 390 °C (Fig. 6g). For the growth time of 90 min, the nanobelts near 445 °C grew longer (Fig. 6j), the nanobelts around 390 °C grew into microbelts (Fig. 6k), and microtowers started to grow near 340 °C (Fig. 6l). Further growth to 120 min is already displayed in Fig. 2b-g with dense 1D structures of different morphologies.

CrystEngComm RSCPublishing

ARTICLE

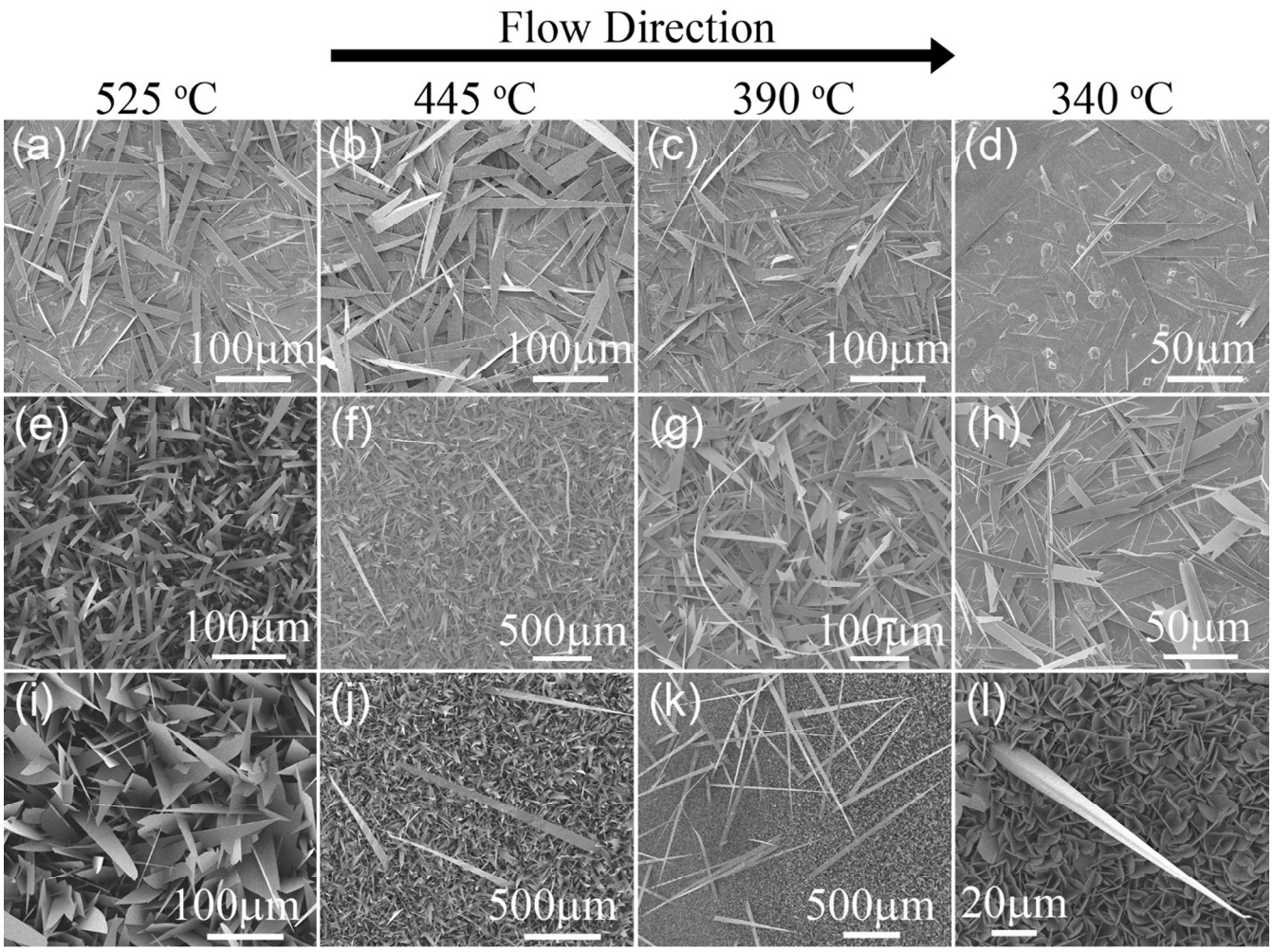

Fig. 6 Growth evolution of the second stage of catalyst-assisted growth of MoO_3 1D structures: SEM images of the deposition at different growth temperatures with growth time of (a-d) 30 min, (e-h) 60 min, and (i-l) 90 min.

To reveal the growth mechanisms for the ultra-long 1D structures in the second stage, specimens were carefully examined to locate and identify the catalyst particles (refer to the Supporting Information for details). Small catalyst particles ranging from several hundred nanometers to several microns were found at different locations of these ultra-long 1D structures (Fig. S2 and S3). Element analysis (Fig. S2 and S3) using EDS confirmed the presence of Na, Mo, and O in these particles, indicating the particles are sodium molybdate catalysts as same as for the growth of forked nanoplates (Fig. 4g and 4j). Thus, the growth of these ultra-long 1D structures was also dominated by the VSS mechanism. Two growth modes were proposed and discussed below for different ultra-long structures.

The ultra-long nanobelts and microbelts follow the same transverse growth mode as the one for the forked nanoplates demonstrated in Fig. 5. Growth steps are illustrated in Fig. **7**a: catalyst particles could nucleate on the forked nanoplates and promote transverse growth of the nanobelts; as the catalyst nucleation and the belt growth continue, nanobelts and microbelts with different dimensions will form depending on the growth temperature and growth time. Figure 7c shows a catalyst particle nucleated at the tip of a forked nanoplate initiating a nanobelt growth. Figures 7d and 7e display catalyst particles located at the middle and the tip of two nanobelts

respectively. It is worth noting that the catalyst particles are always present on the side faces of the belt structures. Even when they are located at the tip of the belt structures, they are on the side faces like the "finger nails". So the growth of the nanobelts and microbelts follows the transverse growth rather than the axial growth. When the belt structures grow into microbelts with micron thickness and millimeter length, dense circular or semicircular nanoflakes (inset of Fig. 2e) grow on top of their side surfaces. This secondary growth on the side surfaces could be attributed to two factors: (1) when the belt structures are so long, stable MoO_3 islands can form on the side surfaces before the oxide species diffuse to the growth front; and (2) as the belt structures grow longer away from the substrate, the local temperature at the belt surface may be lower than the substrate temperature resulting in slower surface diffusion and quicker vapor condensation. On the other hand, the microtower structures follow the axial growth mode in the conventional VSS process. Low growth temperature may be one of the main reasons for the axial growth of microtowers. First, the microtowers in this study primarily grow at the low temperature end of the substrate. And as shown in the Fig. 6l, the microtowers appear later after a thick layer of nanoplates form on the substrate. The growth temperature on top of the nanoplate layer could be even lower than the substrate temperature. With the lower growth temperature, the spreading capability of the Mo oxide species is possibly limited. Thus, based on the analysis of atomic processes shown in Fig. 5c, for the microtower structures the transverse growth via the pathway III is suppressed and axial growth via the pathway II becomes dominant. Hence, the growth steps of the axial growth of microtowers are demonstrated Fig. 7b: catalyst particles form on top of the dense and thick nanoplates and lead to the axial growth at the catalyst-deposition interface; with continuous growth and new nucleation of catalyst particles, tower structures with different heights and morphologies can emerge. Figures 7f, 7g, and 7h show the SEM images of microtowers with a tapered tip, flat top, and a cone shape, respectively.

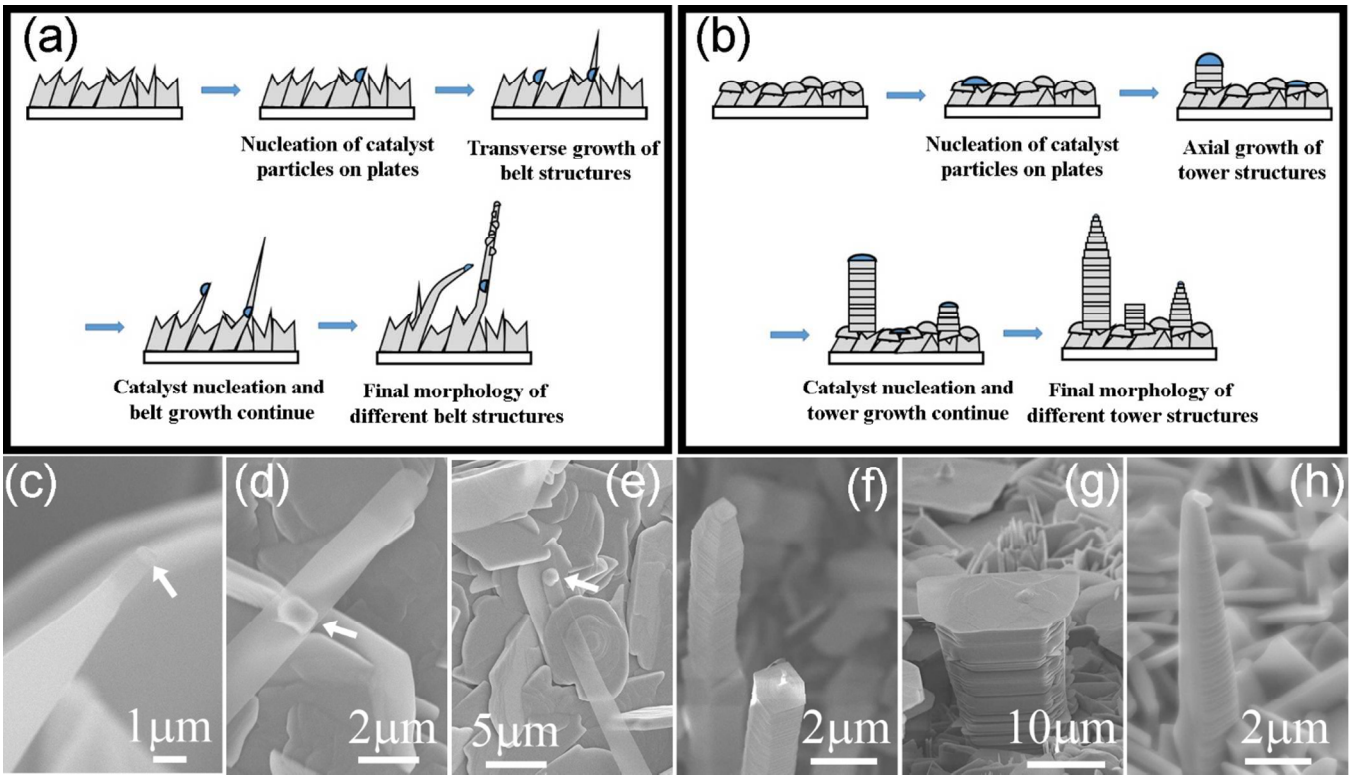

Fig. 7 Schematic illustrations of the VSS growth steps of (a) the transverse mode for MoO_3 nanobelts and microbelts and (b) the axial growth mode for MoO_3 microtowers. (c-e) SEM images of nanobelts showing catalyst particles at different locations: (c) tip of a forked nanoplate, (d) middle of a nanobelt, and (e) tip of a nanobelt. (f-h) SEM images of microtowers with different morphologies: (f) cylinder shape with a tapered tip, (g) flat top, and (h) cone shape.

Above growth modes for the second stage growth of ultra-long nanobelts, microbelts, and microtowers are well supported by the morphology and compositional analyses. However, to further confirm the proposed growth mechanisms, one essential question has to be answered: how can the catalyst particles nucleate on top of the nanoplates? Considering the low melting temperature of $Na_2Mo_4O_{13}$ (~ 522 °C) and the low eutectic temperature of $Na_2Mo_4O_{13}$-MoO_3 system (~ 507 °C), it is possible to produce Na-containing vapors in the reaction chamber especially from the high temperature end of the substrate. The vapors could condense onto the MoO_3 deposition forming catalyst particles and inducing the VSS growth in the second stage. Since no data about $Na_2Mo_4O_{13}$ vapor pressures are available, "side-by-side" growth (refer to the Supporting

Information) was performed to verify above hypothesis. Two substrates, one with NaOH catalyst and one bare substrate, were loaded side-by-side at the same location for the growth (Fig. S4a). To avoid any possible catalyst transports through surface diffusion, the two substrates were separated with a gap of several millimeters. After the growth, besides the non-catalyst rectangular plates, catalyst induced 1D structures (including forked nanoplates, nanobelts, microbelts, and microtowers) were also found on the bare substrate (Fig. S4b-i). This result clearly confirms that the catalyst materials can be evaporated and transferred from the NaOH treated substrate to the untreated one. The catalyst vapors can nucleate and form catalyst particles on the MoO_3 deposition promoting the VSS growth of different 1D structures. It is worth mentioning that catalyst particles were not observed on all the 1D structures. This fact can be explained by following reasons. (1) Catalyst particles can nucleate at any locations along the 1D structures. Some particles may be invisible hiding on the backside of the 1D structures. (2) Because of the evaporation, the catalyst particles may become too small or too thin to be detected. Some particles could even totally disappear terminating the catalyzed growth, which may explain the growth of the microtowers with a flat top (Fig. 2f and Fig. 7g). The evaporation and nucleation of catalyst materials not only promote the growth of the 1D structures in the second stage growth, they also play important roles in shaping the morphologies of these 1D structures. Many 1D structures in the second stage were found to have a tapered shape, such as triangular nanobelts (Fig. 2b and 2d) and microbelts (Fig. 6k), microtowers with tapered tips (Fig. 2f and Fig. 7f) and cone-shaped microtowers (Fig. 7h). Several factors can contribute to the tapering of the 1D structures. First, the reduction in catalyst size may induce the tapering.[37] Due to the evaporation, the size of the catalyst particles can shrink during the growth resulting in the tapered growth. The VS growth on the side surfaces is another possible mechanism,[3b, 38] which promotes the radial growth of the 1D structures forming the tapered shape. Another important factor is the gradually reduced growth during the cooling process. During the cooling, the MoO_3 vapor supply and the growth temperature gradually decrease. Hence the growth rate slows down producing the tapered tips on the top of some 1D structures.

3.3 Different catalysts, hierarchical structures, and optical property

With the similar phase diagrams like the Na_2MoO_4-MoO_3 binary phase diagram, materials contain other alkali metals, such as Li and K,[32] can also be used as catalysts for the growth of MoO_3 1D structures. Experiments have been performed with a variety of alkali metal based materials, including KI, Na_2CO_3, and even alkali metal containing substrates, such as ITO coated glass, glass, and mica. Some selected 1D structures using KI and ITO glass are shown in Fig. 8a and 8b respectively. Other examples are shown in Fig. S5. Based on the modified VSS growth mechanism, hierarchical structures have also been achieved via multiple-growth approaches. Two examples of the hierarchical structures are demonstrated in Fig. 8c-d. Figure 8c shows a specimen grown without catalysts for 120 min followed by a second growth with NaI for 30 min. Assemblies of nanoplates with perpendicular plate surfaces and parallel growth direction were formed. Figure 8d demonstrates another specimen grown with NaOH catalysts for 30 min followed by another growth of 15 min without any additional treatment. The resulting hierarchical structures have a "test-tube-brush" structure with nanoplate branches grown perpendicular around the primary nanoplate stems.

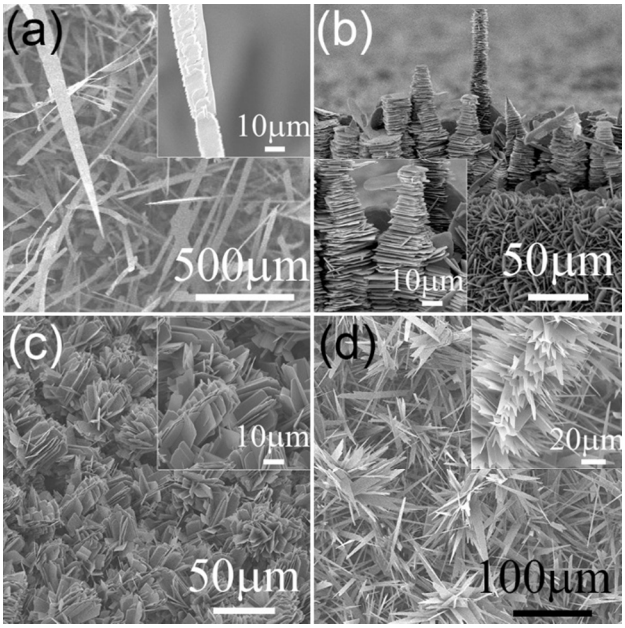

Fig. 8 SEM images of selected MoO_3 1D structures: (a) nanobelts grown with KI and (b) microtowers grown on ITO glass; and (c-d) examples of hierarchical MoO_3 1D structures grown with multiple-growth.

At last, optical property of the MoO_3 deposition was measured using UV-vis spectroscopy. The absorption spectrum is presented in Fig. S6**,** showing that the absorption edge of the MoO_3 crystals obtained in this work, at around 3.0 eV, resembles previous reports on single crystalline and thin film MoO_3 in the literature.[39] The linear fitting (inset of Fig. S6) of the logarithmic plot of the absorbance at the absorption edge indicates a low-energy tail following Urbach's rule, presumably due to bound exciton induced transition and lattice imperfections caused energy band distortion.[39]

4 Conclusions

In summary, MoO_3 1D structures were synthesized using alkali metal based catalysts. The MoO_3 growth was greatly enhanced by the presence of the catalysts forming forked nanoplates and ultra-long 1D structures, such as nanobelts, microbelts, and microtowers. VSS process was identified as the dominant growth mechanism. Different from the conventional catalyst-assisted mechanisms, new transverse growth mode and conventional axial growth mode were discovered. With the

thorough study of the growth evolution, a modified VSS mechanism was proposed based on the strong spreading behavior of MoO_3 material. The proposed mechanism successfully explained the new growth modes. Based on this mechanism, growth of MoO_3 layered 1D structures were realized using a variety of alkali metal based catalysts, and hierarchical structures were achieved by multiple-growth approaches. We believe that the 1D growth using alternative catalysts provides promising opportunities to extend the catalyst-assisted 1D growth to a much broader scope. The growth mechanism revealed here provides a new approach to control the growth direction of 1D structures with respect to the catalyst-deposition axis and can be applied to other layered materials with similar spreading properties as MoO_3.

Acknowledgements

This work was supported by National Science Foundation (DMR-1006547), the start-up fund from the Department of Mechanical Engineering and Engineering Science (MEES) and Charlotte Research Institute at the University of North Carolina at Charlotte (UNC Charlotte), and the faculty research grant from UNC Charlotte. The authors appreciate the Department of MEES and the Center for Optoelectronics and Optical Communications at UNC Charlotte for the support of multiuser facilities. Y. Z. acknowledges the support of Bissell Distinguished Professorship.

Notes and references

[a] Department of Physics and Optical Science, and Optical Science and Engineering Program, The University of North Carolina at Charlotte, 9201 University City Boulevard, Charlotte, NC 28223, USA.
[b] Department of Mechanical Engineering and Engineering Science, The University of North Carolina at Charlotte, 9201 University City Boulevard, Charlotte, NC 28223, USA.
[c] School of Materials Science and Engineering, Southwest Jiaotong University, No. 111, North 1st Section of Second Ring Road, Chengdu, Sichuan 610031, P.R. China.
[d] Department of Electrical and Computer Engineering, The University of North Carolina at Charlotte, 9201 University City Boulevard, Charlotte, NC 28223, USA
[*] Email address: hzhang3@uncc.edu

Electronic Supplementary Information (ESI) available: additional SEM, EDS, and Raman data, results from control experiments, and UV-Vis measurement. See DOI: 10.1039/b000000x/

1. (a) R. S. Wagner and W. C. Ellis, *Appl. Phys. Lett.*, 1964, **4**, 89; (b) E. I. Givargizov, *J. Cryst. Growth*, 1975, **31**, 20.
2. (a) C. M. Lieber, *Solid State Commun.*, 1998, **107**, 607; (b) M. Law, J. Goldberger and P. D. Yang, *Ann. Rev. Mater. Res.*, 2004, **34**, 83; (c) Y. N. Xia, P. D. Yang, Y. G. Sun, Y. Y. Wu, B. Mayers, B. Gates, Y. D. Yin, F. Kim and Y. Q. Yan, *Adv. Mater.*, 2003, **15**, 353; (d) H. J. Fan, P. Werner and M. Zacharias, *Small*, 2006, **2**, 700.
3. (a) T. I. Kamins, R. S. Williams, D. P. Basile, T. Hesjedal and J. S. Harris, *J. Appl. Phys.*, 2001, **89**, 1008; (b) Y. Wang, V. Schmidt, S. Senz and U. Goesele, *Nat. Nanotechnol.*, 2006, **1**, 186; (c) J. L. Lensch-Falk, E. R. Hemesath, D. E. Perea and L. J. Lauhon, *J. Mater. Chem.*, 2009, **19**, 849.
4. (a) H. F. Yan, Y. J. Xing, Q. L. Hang, D. P. Yu, Y. P. Wang, J. Xu, Z. H. Xi and S. Q. Feng, *Chem. Phys. Lett.*, 2000, **323**, 224; (b) L. W. Yu, P. J. Alet, G. Picardi and P. R. I. Cabarrocas, *Phys. Rev. Lett.*, 2009, **102**; (c) H. Chandrasekaran, G. U. Sumanasekara and M. K. Sunkara, *J. Phys. Chem. B*, 2006, **110**, 18351.
5. (a) T. J. Trentler, K. M. Hickman, S. C. Goel, A. M. Viano, P. C. Gibbons and W. E. Buhro, *Science*, 1995, **270**, 1791; (b) T. Hanrath and B. A. Korgel, *J. Am. Chem. Soc.*, 2002, **124**, 1424.
6. (a) J. D. Holmes, K. P. Johnston, R. C. Doty and B. A. Korgel, *Science*, 2000, **287**, 1471; (b) F. M. Davidson, R. Wiacek and B. A. Korgel, *Chem. Mater.*, 2005, **17**, 230.
7. (a) H. Y. Tuan, D. C. Lee, T. Hanrath and B. A. Korgel, *Nano Lett.*, 2005, **5**, 681; (b) S. Barth, M. M. Kolesnik, K. Donegan, V. Krstic and J. D. Holmes, *Chem. Mater.*, 2011, **23**, 3335.
8. Z. W. Pan, Z. R. Dai, C. Ma and Z. L. Wang, *J. Am. Chem. Soc.*, 2002, **124**, 1817.
9. Z. W. Pan, S. Dai, C. M. Rouleau and D. H. Lowndes, *Angew. Chem.-Int. Edit.*, 2005, **44**, 274.
10. J. Wang, K. Chen, M. Gong, B. Xu and Q. Yang, *Nano Lett.*, 2013.
11. K. W. Kolasinski, *Curr. Opin. Solid State Mat. Sci.*, 2006, **10**, 182.
12. (a) S. A. Fortuna, J. Wen, I. S. Chun and X. Li, *Nano Lett.*, 2008, **8**, 4421; (b) S. Li, X. Huang, Q. Liu, X. Cao, F. Huo, H. Zhang and C. L. Gan, *Nano Lett.*, 2012, **12**, 5565; (c) Z. Zhang, L. M. Wong, H. X. Wang, Z. P. Wei, W. Zhou, S. J. Wang and T. Wu, *Adv. Funct. Mater.*, 2010, **20**, 2511.
13. (a) F. Cora, A. Patel, N. M. Harrison, C. Roetti and C. R. A. Catlow, *J. Mater. Chem.*, 1997, **7**, 959; (b) M. Chen, U. V. Waghmare, C. M. Friend and E. Kaxiras, *J. Chem. Phys.*, 1998, **109**, 6854.
14. J. N. Yao, K. Hashimoto and A. Fujishima, *Nature*, 1992, **355**, 624.
15. P. E. Sheehan and C. M. Lieber, *Science*, 1996, **272**, 1158.
16. Y. Chen, C. Lu, L. Xu, Y. Ma, W. Hou and J.-J. Zhu, *CrystEngComm*, 2010, **12**, 3740.
17. (a) E. Comini, L. Yubao, Y. Brando and G. Sberveglieri, *Chem. Phys. Lett.*, 2005, **407**, 368; (b) A. M. Taurino, A. Forleo, L. Francioso, P. Siciliano, M. Stalder and R. Nesper, *Appl. Phys. Lett.*, 2006, **88**, 152111; (c) X. Sha, L. Chen, A. C. Cooper, G. P. Pez and H. Cheng, *J. Phys. Chem. C.*, 2009, **113**, 11399; (d) S. Choopun, P. Mangkorntong, P. Subjareon, N. Mangkorntong, H. Tabata and T. Kawai, *Jpn. J. Appl. Phys.*, 2004, **43**, L91 LP.
18. L. Q. Mai, B. Hu, W. Chen, Y. Y. Qi, C. S. Lao, R. S. Yang, Y. Dai and Z. L. Wang, *Adv. Mater.*, 2007, **19**, 3712.
19. S. Hariharan, K. Saravanan and P. Balaya, *Electrochem. Commun.*, 2013, **31**, 5.
20. (a) X.-L. Li, J.-F. Liu and Y.-D. Li, *Appl. Phys. Lett.*, 2002, **81**, 4832; (b) T. Xia, Q. Li, X. Liu, J. Meng and X. Cao, *J. Phys. Chem. B*, 2006, **110**, 2006; (c) G. Li, L. Jiang, S. Pang, H. Peng and Z. Zhang, *J. Phys. Chem. B*, 2006, **110**, 24472; (d) G. A. Camacho-Bragado and M. Jose-Yacaman, *Appl. Phys. A*, 2006, **82**, 19.
21. (a) H. C. Zeng, *J. Cryst. Growth*, 1998, **186**, 393; (b) J. Li, P. Wei, J. Chen and L. Rongti, *J. Am. Ceram. Soc.*, 2002, **85**, 2116; (c) Y. B. Li, Y. Bando, D. Golberg and K. Kurashima, *Appl. Phys. Lett.*, 2002, **81**, 5048; (d) J. Zhou, S. Z. Deng, N. S. Xu, J. Chen and J. C. She, *Appl. Phys. Lett.*, 2003, **83**, 2653; (e) P. Badica, *Cryst. Growth Des.*, 2007, 2; (f) B. Yan, Z. Zheng, J. Zhang, H. Gong, Z. Shen, W. Huang and T. Yu, *J. Phys. Chem. C*, 2009, 20259.
22. L. Cai, P. M. Rao and X. Zheng, *Nano Lett.*, 2011, **11**, 872.

23. (a) H. Zhang, T. T. Xu, M. Tang, T.-h. Her and S.-y. Li, *J. Vac. Sci. Technol. B*, 2010, **28**, 310; (b) T. Sheng, P. P. Chavvakula, B. Cao, N. Yue, Y. Zhang and H. Zhang, *J. Cryst. Growth*, 2014, **395**, 61.
24. K. Kalantar-zadeh, J. Tang, M. Wang, K. L. Wang, A. Shailos, K. Galatsis, R. Kojima, V. Strong, A. Lech and R. B. K. De, *Nanoscale*, 2010, 429.
25. D. E. Diaz-Droguett, A. Zuniga, G. Solorzano and V. M. Fuenzalida, *J. Nanopart. Res.*, 2012, **14**, 679.
26. F. Cora, A. Patel, N. M. Harrison, C. Roetti and C. Richard A. Catlow, *J. Mater. Chem.*, 1997, **7**, 959.
27. Z. R. Dai, Z. W. Pan and Z. L. Wang, *Adv. Funct. Mater.*, 2003, **13**, 9.
28. G. V. Samsonov, ed., *The Oxide Handbook*, IFI/Plenum, New York, 1973.
29. (a) G. D. Saraiva, W. Paraguassu, M. Maczka, P. T. C. Freire, F. F. de Sousa and J. Mendes Filho, *J. Raman Spectrosc.*, 2011, **42**, 1114; (b) V. V. Fomichev, M. E. Poloznikova and O. I. Kondratov, *Russ. Chem. Rev.*, 1992, **61**, 877; (c) K. Schofield, *Energy Fuels*, 2005, **19**, 1898; (d) K. Eda, *J. Solid State Chem.*, 1991, **95**, 64; (e) W. G. Chu, L. N. Zhang, H. F. Wang, Z. H. Han, D. Han, Q. Q. Li and S. S. Fan, 2007, **22**; (f) T. Siciliano, a. Tepore, E. Filippo, G. Micocci and M. Tepore, *Mater. Chem. Phys.*, 2009, **114**, 687.
30. G. A. El-Shobaky, G. A. Fagal and N. A. Hassan, *Thermochim. Acta*, 1998, **311**, 205.
31. J. Goldstein, *Scanning electron microscopy and x-ray microanalysis*, Kluwer Academic/Plenum Publishers, New York, 2003.
32. (a) E. M. Levin, *Phase diagrams for ceramists*, American Ceramic Society, Columbus, Ohio, 1956; (b) F. Hoermann, *Z. Anorg. Allg. Chem.*, 1929, **177**, 145.
33. V. P. Yurkinskii, E. G. Firsova and S. A. Proskura, *Russ. J. Appl. Chem.*, 2005, **78**, 360.
34. K. Subannajui, N. Ramgir, R. Grimm, R. Michiels, Y. Yang, S. Muller and M. Zacharias, *Cryst. Growth Des.*, 2010, **10**, 1585.
35. (a) J. Leyrer, D. Mey and H. Knözinger, *J. Catal.*, 1990, **124**, 349; (b) S. Gunther, M. Marsi, A. Kolmakov, M. Kiskinova, M. Noeske, E. Taglauer, G. Mestl, U. A. Schubert and H. Knozinger, *J. Phys. Chem. B*, 1997, **101**, 10004; (c) W. M. Xu, J. F. Yan, N. Z. Wu, H. X. Zhang, Y. C. Xie, Y. Q. Tang and Y. F. Zhu, *Surf. Sci.*, 2000, **470**, 121; (d) Z. Song, T. Cai, Z. Chang, G. Liu, J. A. Rodriguez and J. Hrbek, *J. Am. Chem. Soc.*, 2003, **125**, 8059; (e) S. Gunther, L. Gregoratti, M. Kiskinova, E. Taglauer, P. Grotz, U. A. Schubert and H. Knozinger, *J. Chem. Phys.*, 2000, **112**, 5440.
36. (a) H. Qi, C. Wang and J. Liu, *Adv. Mater.*, 2003, **15**, 411; (b) K. Q. Hong, W. C. Yin, H. S. Wu, J. Gao and M. H. Xie, *Nanotechnology*, 2005, **16**, 1608; (c) R. Hu, H. Wu and K. Hong, *J. Mater. Res.*, 2009, **24**, 187.
37. (a) J. B. Hannon, S. Kodambaka, F. M. Ross and R. M. Tromp, *Nature*, 2006, **440**, 69; (b) E. J. Schwalbach and P. W. Voorhees, *Nano Lett.*, 2008, **8**, 3739.
38. S. S. Amin, A. W. Nicholls and T. T. Xu, *Nanotechnology*, 2007, **18**.
39. (a) S. K. Deb, *Proc. R. Soc. London, Ser. A*, 1968, **304**, 211; (b) M. Itoh, K. Hayakawa and S. Oishi, *J. Phys.: Condens. Matter*, 2001, **6853**.

Graphical Abstract

New Growth Modes of Layered Molybdenum Oxide 1D Structures using Alternative Catalysts: Transverse Mode vs. Axial Mode

Tao Sheng,[a] Baobao Cao,[bc] Yong Zhang,[d] and Haitao Zhang[*b]

[a] *Department of Physics and Optical Science, and Optical Science and Engineering Program, The University of North Carolina at Charlotte, 9201 University City Boulevard, Charlotte, NC 28223, USA*

[b] *Department of Mechanical Engineering and Engineering Science, The University of North Carolina at Charlotte, 9201 University City Boulevard, Charlotte, NC 28223, USA*

[c] *School of Materials Science and Engineering, Southwest Jiaotong University, No. 111, North 1st Section of Second Ring Road, Chengdu, Sichuan 610031, P.R. China*

[d] *Department of Electrical and Computer Engineering, The University of North Carolina at Charlotte, 9201 University City Boulevard, Charlotte, NC 28223, USA*

Email address: hzhang3@uncc.edu

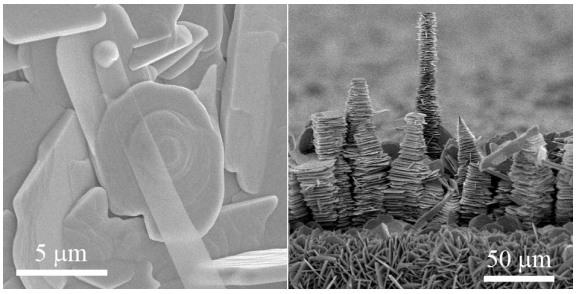

Both transverse and axial growth modes were discovered in the CVD synthesis of molybdenum oxide (MoO_3) 1D structures using alkali metal based catalysts. A modified vapor-solid-solid (VSS) mechanism was proposed.